Exploring the application of neural networks in predictions of nuclear binding energies.

Thesis Submitted for Degree of Bachelor of Science

Project Duration: 3.5 Months

Supervised by: Gillis Carlsson and Andrea Idini

Martin Waites

LUND
UNIVERSITY

Department of Physics

Division of Mathematical Physics

Spring 2020

ACKNOWLEDGEMENTS

I would like to begin by thanking my supervisors Gillis Carlsson and Andrea Idini for for being available to offer assistance whenever difficulties arose and for providing helpful feedback. Additionally I would like to thank a previous master student Weiyi Cui for assistance introducing me to some of the computer science aspects of this work. Finally I would like to thank my grandparents for their calming presence, and my parents for their assistance with both maintaining stress and providing advice.

ABSTRACT

In this project the locations of the proton and neutron drip-lines are predicted using neural networks and theoretical data obtained by applying the HFBTHO program [19]. For each of the neural networks a comparison is made between neural network predictions and experimental data in the region experimental data exists. By comparing the effectiveness of the networks at reproducing experimental results with the effectiveness of the HFBTHO program it is found that extensive improvements can be made these results. This indicates that the application of machine learning exists as a potential method for making corrections to theoretical modes. Whether the final predictions are sufficiently trustworthy to reach a conclusion is difficult to determine however this seems to be a potential path for future development into obtaining data.

CONTENTS

1 INTRODUCTION

In recent years, along with the discovery of new elements, there has been a renewed interest in the properties of nuclei in the super heavy and exotic regions of the nuclear chart. These properties are the focus of many studies within the fields of atomic physics, chemistry and nuclear physics where attempts are made to determine the chemical and physical properties of these less understood nuclei. The difficulty of performing experimental studies on nuclei with short half lives makes the application of theoretical models the main approach for determining properties of interest. Within nuclear physics one of the main properties of interest is the nuclear binding energy of each nucleus, as binding energy provides information about it's relative stability. An issue with theoretical approaches within nuclear physics is that the approximated errors of values obtained experimentally for nuclear binding energies are orders of magnitude better than what is obtained from theoretical models [10]. The application of Neural networks and other methods of Machine learning, with their continued advancement, exist as a potential method of providing corrections to the theoretically determined values in order to bridge this gap.

This work will focus on exotic nuclei and the application of neural networks in determining the position of the neutron and proton drip-lines. The drip-lines designate the limit of nuclear stability and occur when the nucleus goes from requiring energy to remove nucleons to producing energy when they are removed, as such any nucleus beyond the drip-line will decay immediately. The topic of exotic nuclei specifically has become a focus recently with experimental results from recently built Radioactive isotope beam facilities such as RIBF at RIKEN involving exploration of neutron halo structure using breakup reactions[21]. Neutron halo structure refers to a nucleus structure consisting of a central nucleus with orbiting more loosely bound neutrons. Other similar experiments concerning exotic nuclei are being performed or planned at SPIRAL2 at GANIL in France[6], FAIR at GSI in Germany and FRIB at MSU in the USA. With continued experimental studies it remains important to have predictions for the drip-line location in order to plan future experiments and expand knowledge concerning possible locations of the drip-line.

This report is structured such that section 2 (Theory and Background) will first explain the basics of neural networks, followed by some of the general properties of nuclei and discovered properties unique to exotic nuclei including the method of determining the location

of the neutron drip-line. Section 2 will then go on to explain the model used in this work to obtain theoretical results for properties of nuclei. Section 3 will then describe the method by specifying the parameters used for the HFBTHO program. Section 4 then presents and discusses results obtained through the different methods applied, including a basic neural network result, theoretical model results and the results of neural networks trained by applying information obtained from the theoretical model. This is followed by section 5, concluding the report and considering potential future directions for study. Additionally in appendix A and B the specific neural network setup used in this work and additional information concerning HFBTHO parameters can be found respectively.

2 THEORY AND BACKGROUND

2.1 Neural Networks

A neural network is a method of Machine learning which functions using several interconnected nodes organised into layers. The name originates from the resemblance to a brain with it's connected neurons. As visible in figure 2 a neural network is structured such that it starts with an input layer followed by a number of hidden layers and ends in an output layer.

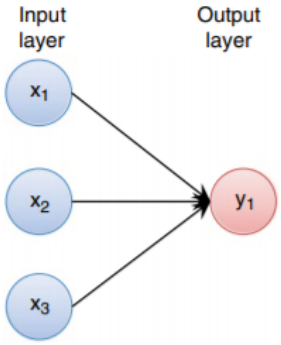

FIG. 1: Basic representation of a neural network with three input nodes no hidden layers and one output node, From [3]

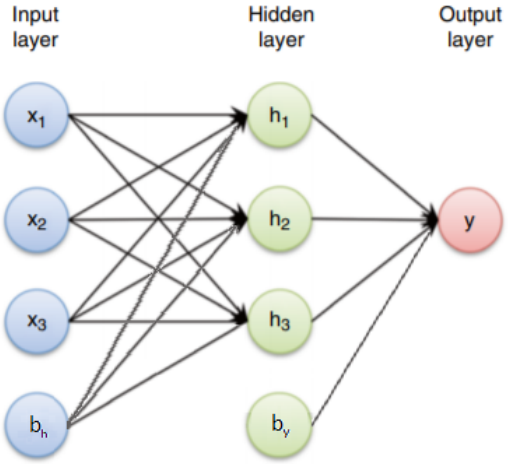

FIG. 2: Basic representation of a neural network with three input nodes one hidden layer with three nodes and one output node, From [3]

The value of each node can be determined by calculating the weighted sum of nodes connected behind it, with each layer modified by an activation function. This could be visualised by considering each arrow in figures 1 and 2 to be the application of a weight to the value of the originating node. The value of the output node of Figure 1 is by this method expressed by:

$$y = \psi\left(\sum_i w_i x_i\right) \tag{1}$$

where w_i are the weights applied to the input values x_i and ψ is the activation function of the neural network which maps the weighted sum to the output. For a more complicated system each layer will have a bias and there will be multiple sums, Figure 2 requires the

expression:

$$y = b_y + \sum_j w_j \psi \left(b_{h,j} + \sum_i w_{i,j} x_i \right), \tag{2}$$

where b_y is the bias to the output node, $w_{h,j}$ are the weights for the hidden layer nodes, $b_{h,j}$ are the biases to the hidden layer nodes, and $w_{x,i,j}$ are the input layer weights to the hidden layer nodes. The output of these expressions is the prediction of the network. Improving the predictions is done by comparison to a target set where a loss score determined using:

$$Score = \sum_i (y_i - t_i)^2, \tag{3}$$

where t_i are the target values. This loss score is a measure of the quality of the prediction and is used by an optimizer to improve the neural network. The optimizer works to minimize the loss score by adjusting the weights in the neural network. The network is then run with the new weights gaining a new loss score, where this process is repeated until a satisfactory loss score is achieved.

In order to further improve the neural network an additional method called cross validation can be applied. This method splits the target and input sets into a number of smaller sets, several networks are then trained, where each network is trained on all but one of the smaller sets. After the networks are trained they make predictions on the remaining set and obtain a prediction score for their effectiveness on a set were they where not trained. The network with the best prediction score is then taken as the final model. This set division can be visualised in table I.

Full set:	set 1	set 2	set 3	set 4	set 5	set 6
run 1:	set 1	set 2	set 3	set 4	set 5	test set
run 2:	set 1	set 2	set 3	set 4	test set	set 6
run 3:	set 1	set 2	set 3	test set	set 5	set 6
run 4:	set 1	set 2	test set	set 4	set 5	set 6
run 5:	set 1	test set	set 3	set 4	set 5	set 6
run 6:	test set	set 2	set 3	set 4	set 5	set 6

TABLE I: Visualisation of input and test data division for multiple runs of a cross validation method of neural network improvement.

The advantage of cross validation in this work is that it is a method of optimising based on the effectiveness of the network at making predictions outside the set where the network is trained. As this work will focus on extrapolation into the exotic region of the nuclear chart this improvement in predictions outside the trained set is crucial.

2.2 Nuclear Basics

There exist multiple methods for approximating the properties of the nucleus in order to make effective nuclear models. This work relies on the Hartree-Fock-Bogolyubov method, a self-consistent mean field theory approach explained in a later chapter. A more commonly used model is the nuclear shell model. However, it is important to understand why approximations are necessary in the first place. Ideally the structure and dynamics of atomic nuclei could be described on the basis of the fundamental underlying theory of the strong interaction, quantum chromodynamics (QCD). The issue that arises is that the protons and neutrons that make up the nucleus are complex systems constructed from quarks and gluons. While free nucleon-nucleon interactions can be measured experimentally and are well described theoretically, inside an atomic nucleus the interaction between two nucleons changes based on the presence and locations of other nucleons in the system. This leads to a necessity of using effective interactions to describe the interactions between protons and neutrons in an atomic nucleus. The strong interaction between nucleons is a van der Waals like interaction that governs a two-component quantum many-body system. Direct analytical calculations of such systems are currently not possible [15].
In the nuclear shell model the basic idea is to approximate the potential part of the Hamiltonian for the Schrödinger equation of the system of nucleons that makes up the nucleus with a central potential. This approximation gives rise to groups of energy levels referred to as shells which are filled following the Pauli exclusion principle. In order to determine values for nuclear properties of nuclei one needs a method of determining the Hamiltonian and solving the Schrodinger equation of the system. In a simplified scenario where we restrict discussion to one and two-body interactions we can solve the Schrodinger equation of the system by splitting the Hamiltonian of the system into a one particle H_1 and two particle H_2 operator. The one particle operator consists of the kinetic energy of the system along with the central potential. The two particle operator then represents the interactions between

nucleons in the N-body system giving a Hamiltonian as shown in equation (4).

$$H = H_1 + H_2 = \sum_{i=1}^{N} \left[-\frac{\hbar^2}{2m} \nabla_i^2 + V(r) \right] + \sum_{i \neq j}^{N} V(\vec{r}_i, \vec{r}_j) \tag{4}$$

From here there are multiple methods to continue, including the configuration interaction method and the self-consistent mean field approach. The configuration interaction method expresses the wavefunction as a combination of Slater determinants [24]. Solving this for a many body problem then requires expansion of the wavefunction into a mixed states basis. This means solving a matrix of Slater determinants the dimensions of this matrix growing rapidly with an increase in nucleons involved. In general the Hamiltonian in (4) is not sufficient and requires additional many-nucleons interaction terms, for example the original Skyrme formulation considered a 3 body contact interaction, that was then reduced to a density dependent two-body interaction in the case of even-even nuclei[11].

2.3 Exotic Nuclei

Exotic nuclei are nuclei with a high ratio of neutrons to protons, or protons to neutrons when compared to stable nuclei. These ratios result in the nuclei having different properties and nuclear structure from non exotic nuclei. Two examples of this in the neutron drip-line region where nuclei have a large ratio of neutrons compared to protons are neutron skins and neutron halos, where the nuclei have a skin of neutrons around a central nucleus or loosely bound orbiting neutrons respectively.

"Neutron skin" refers to the broader distribution of neutrons when compared to protons in nuclei with a high ratio of neutrons. The effect occurs due to a distribution of neutrons and protons symmetrically according to the amount of each nucleon type being energetically favorable [20]. The thickness of the neutron skin can be represented by the difference:

$$\sqrt{\langle r^2 \rangle_n} - \sqrt{\langle r^2 \rangle_p} \tag{5}$$

where $\sqrt{\langle r^2 \rangle_a}$ $(a = n, p)$ represents the root mean square standard deviation of a point like particle a from the centre of the nucleus. The existence of neutron skin has been observed experimentally for ^{6}He and ^{8}He using high-energy radioactive nuclear beams[12]. For these isotopes specifically the neutron skin thickness has been found to be $\approx 0.9fm$ [26]. These results and the accounting for neutron skin is important due to its effect on the slope

parameter of the symmetry energy[12], a parameter of particular importance concerning the equation-of-state of neutron-star matter [16].

Another interesting property of exotic nuclei in the same region is the neutron halo. In the region of the neutron drip-line ^{11}Li was discovered to have a far greater matter radius than what is expected based on the scaling of nuclear mass radii for stable nuclei. Stable nuclei in general have a mass radius that scales as $A^{1/3}$, where A is the mass number while ^{11}Li had a mass radius around 30% greater than expected[14]. Neutron halos were discovered through an interaction cross section based experiment and the result for ^{11}Li suggested "a large deformation or a long tail in the matter distribution"[25]. There exist both single neutron and multiple neutron halos and both cases are caused by loosely bound valence neutrons moving in an extended region around the core nucleus[7].

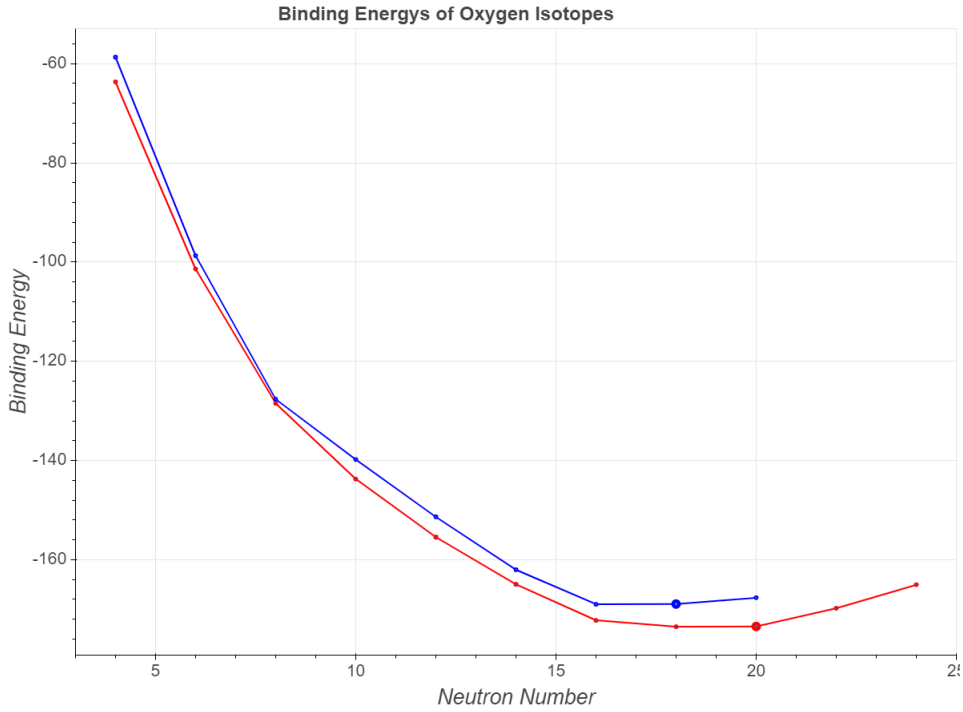

FIG. 3: Demonstration of the method for determining the drip-line location, the two large dots indicating the location determined for two neutron the drip-line. The blue line is produced using experimental data while the red line is theoretical predictions produced by the HFBTHO program.

The neutron drip-line itself is the limit of nuclear stability in the neutron direction. The one neutron drip-line is intrinsically connected with the separation energy of a single neutron (S_{1n}). In terms of binding energy the one neutron drip-line occurs when $S_{1n}(N, Z) =$

$B(Z, N-1) - B(Z, N)$ is approximately zero[13], where $B(Z, N)$ is the binding energy of the nucleus with proton number Z and neutron number N. This can be considered to be the point at which the nucleus goes from gaining total binding energy to losing total binding energy when a neutron is added to the nucleus. At such a point it would be energetically favorable to immediately emit the new neutron causing the nucleus to "drip" neutrons when additional neutrons are added. The limitations of the program applying the theoretical model in this work restricts us to only considering even-even nuclei leading our investigation to be about the location of the two neutron drip-line. Similarly to the one neutron drip-line this occurs when $S_{2n}(N, Z) = B(Z, N-2) - B(Z, N)$ is approximately zero shown in figure 3. The advantage of the two neutron drip-line over the one neutron drip-line is the one neutron drip-line occurs earlier and there can exist stable nuclei beyond the one neutron drip-line. This occurs due to even-even nuclei having higher binding energy than even-odd nuclei in general, an example of this is helium where ^{6}He and ^{8}He are orders of magnitude more stable than both ^{5}He and ^{7}He. The two neutron drip-line then more accurately signifies the point after which there are no stable nuclei.

2.4 Hartree-Fock-Bogolyubov

The program applied to obtain theoretical properties of the investigated nuclei is the HF-BTHO program. This program finds the "Axially Deformed Solution of the Skyrme-Hartree-Fock-Bogolyubov Equations using The Transformed Harmonic Oscillator Basis" [19][18]. As such the theoretical model central to this work is the Hartree-Fock-Bogolyubov model.

2.4.1 Hartree-Fock Method

The Hartree-Fock Method introduced by D. Hartree, V. Fock and J. C. Slater was developed with the goal of approximating the ground state properties of a general N-body problem in Quantum Physics. The original main application of this method was the study of the Coulomb Hamiltonian consisting of electrons interacting with static nuclei within atomic physics. When applying this method to nuclear physics one again begins with the Hamiltonian, in this case an A-body Hamiltonian with A being $A = N + Z$ the sum of the number of neutrons N and the number of protons Z. This A-body Hamiltonian H can be

expressed as shown in equation 6

$$H = -\frac{\hbar^2}{2m}\sum_{i=1}^{A}\Delta_i + \sum_{i<j}V(x_i - x_j) \tag{6}$$

where $\hbar$ is the Planck constant, m is the mass of the nucleon here the approximation neglects the minor difference in mass between protons and neutrons in order to simplify the expression, Δ_i is the Laplacian with respect to the x_i variables, V is the given potential and the points $x_i (1 \leq i \leq A)$ are generic points on $\mathbb{R}^3$.

The Hamiltonian H is an operator acting on the closed subspace $\mathscr{H}$ consisting of anti-symmetric functions Φ of $x = (x_1, ..., x_A) \in (\mathbb{R}^3)^A$ such that:

$$\Phi(x_{\sigma(1)}, ..., x_{\sigma(A)}) = (-1)^{|\sigma|}\Phi(x_1, ..., x_A) \tag{7}$$

for all $x_i \in \mathbb{R}^3 (1 \leq i \leq A)$ and for all permutations σ of $\{1, ..., A\}$, here $|\sigma|$ represents the signature of σ. In order to determine the ground state of this A-body system one considers that the ground state can be found with equation (8)[17]:

$$E = \text{Inf}\left\{(H\Phi, \Phi)_{L^2}/\Phi \in \mathscr{H}, \int_{(\mathbb{R}^3)^A}|\Phi|^2 dx = 1\right\} \tag{8}$$

In nuclear physics it's important to consider nuclei with large A where one cannot directly compute equation (8). A suggested approximation by Hartree [8] was to consider wavefunctions Ψ in the form:

$$\Phi(x_1, ..., x_A) = \prod_{i=1}^{A}\psi_i(x_i) \tag{9}$$

Since this equation does not satisfy the symmetry constraint (7) V. Fock and J. C. Slater suggested the better choice of Φ as:

$$\Phi(x_1, ..., x_A) = \frac{1}{\sqrt{A!}}\sum_{\sigma}(-1)^{|\sigma|}\prod_{i=1}^{A}\psi_{\sigma(i)}(x_i) = \frac{1}{\sqrt{A!}}det(\psi_i(x_j)) \tag{10}$$

With this approximation and the expression for the ground state in (8) one can obtain the following expression for the Hartree-Fock ground state.

$$E = \text{Inf}\left\{E(\psi_i, ..., \psi_A)/\psi_i \in L^2(\mathbb{R}^3), \int_{\mathbb{R}^3}\psi_i\psi_j^* dx = \delta_{ij} \text{ for } 1 \leq i, j \leq A\right\} \tag{11}$$

where [17]:

$$E(\psi_i, ..., \psi_A) = \frac{\hbar^2}{2m}\sum_{i=1}^{A}\int_{\mathbb{R}^3}|\nabla\psi_i|^2 dx + \frac{1}{2}\sum_{i,j}\int_{\mathbb{R}^3\times}\int_{\mathbb{R}^3}|\psi_i(x)|^2 V(x-y)|\psi_j(y)|^2 dxdy$$
$$- \frac{1}{2}\sum_{i,j}\int_{\mathbb{R}^3\times}\int_{\mathbb{R}^3}\psi_i(x)\psi_j^*(x)V(x-y)\psi_i^*(y)\psi_j(y)dxdy \tag{12}$$

This equation can be expressed in terms of density matrix[17]:

$$E(\psi_i, ..., \psi_A) = \frac{\hbar^2}{2m}\int_{\mathbb{R}^3} \tau dx + \frac{1}{2}\int_{\mathbb{R}^3\times}\int_{\mathbb{R}^3} \rho(x)V(x-y)\rho(y)dxdy \\ - \frac{1}{2}\int_{\mathbb{R}^3\times}\int_{\mathbb{R}^3} V(x-y)|\rho(x,y)|^2 dxdy \quad (13)$$

where $\tau(x)$ is the density of the kinetic energy given by $\tau = \sum_{i=1}^{A} |\nabla\psi_i|^2$, $\rho(x)$ is the density given by $\rho = \sum_{i=1}^{A} |\psi_i(x)|^2$ and $\rho(x,y)$ is the density matrix given by $\rho(x,y) = \sum_{i=1}^{A} \psi_i(x)\psi_i^*(y)$. In both cases the second and third terms are generally referred to as the direct term and the exchange term respectively. The density matrix form in equation (13) is interesting as it shows that the energy of the A-body system can be expressed as a functional of the density matrix in a way that is similar to the density functional theory.

2.4.2 Bogolyubov Transformation

The Bogolyubov Transformation is a method of including pairing correlations through the concept of independent quasiparticles. In a mean-field model like the one considered in the Hartree-Fock Method one has a set of single-nucleon wave functions[1].

$$\{\psi_i(\vec{x}), i = 1, ..., N\}, \vec{x} = (\vec{r}, s, o) \quad (14)$$

Where $\vec{r}$ is the position in spacial coordinate, s is the spin index and o is the isospin index of the nucleon, and $N > A$ is the number of single particle wavefunctions larger than the number of nucleons. Here creation and annihilation operators are introduced $\hat{a}_i^+$ and $\hat{a}_i$ respectively for a nucleon in the single-particle state $\psi_i(\vec{x})$ expressed with:

$$\hat{a}_i^+ = \int d^3r \sum_{so} \psi_i(\vec{x})\hat{a}_x^+ \quad (15)$$

where $\hat{a}_x^+$ is the creation operator for eigenstates of nucleon position. Considering the independent-particle model where the state of the nucleus is described by the Slater determinant $|\Phi\rangle = det\{\psi_i(\vec{x}), i = 1, ..., A\}$ one can use these operators to formally characterise the independent-particle by $\hat{a}_i^+ |\Phi\rangle = 0$ and $\hat{a}_i |\Phi\rangle = 0$ for $i = 1, ..., A$ for occupied and and unoccupied states respectively. The Bogolyubov transformation then defines independent quasiparticles as[19]:

$$b_k = \sum_i \left(U_{ik}^* a_i + V_{ik}^* a_i^+\right), \text{ and } b_k^+ = \sum_i \left(V_{ik} a_i + U_{ik} a_i^+\right) \quad (16)$$

connecting single particle states to quasiparticle states. In matrix form equation (16) can be rewritten as:

$$\begin{pmatrix} b \\ b^+ \end{pmatrix} = \begin{pmatrix} U^+ & V^+ \\ V^T & U^T \end{pmatrix} \begin{pmatrix} a \\ a^+ \end{pmatrix} \tag{17}$$

where in both cases the matrices U and V satisfy the relations [19]:

$$U^+U + V^+V = I, \;\; UU^+ + V^*V^T = I, \;\; U^TV + V^TU = 0, \;\; UV^+ + V^*U^T = 0 \tag{18}$$

2.4.3 Hartree-Fock-Bogolyubov equations

The Hartree-Fock-Bogolyubov method begins by considering a two-body Hamiltonian in terms of the annihilation and creation operators of a system of fermions:

$$H = \sum_{i_1 i_2} e_{i_1 i_2} a^+_{i_1} a_{i_2} + \frac{1}{4} \sum_{i_1 i_2 i_3 i_4} \bar{v}_{i_1 i_2 i_3 i_4} a^+_{i_1} a^+_{i_2} a_{i_3} a_{i_4} \tag{19}$$

where $\bar{v}_{i_1 i_2 i_3 i_4} = \langle i_1 i_2 | V | i_3 i_4 - i_4 i_3 \rangle$ are anti-symmetrized two-body interaction matrix elements. With the Hartree-Fock-Bogolyubov method the ground state wave function $|\Phi\rangle$ is defined as the quasiparticle vacuum $b_k |\Phi\rangle = 0$ [19]. The expectation value of the Hamiltonian in (19) can then be expressed as an energy functional in terms of the normal one-body density matrix ρ and the pairing one-body density matrix κ:

$$\rho_{ii'} = \left\langle \Phi | a^+_{i'} a_i | \Phi \right\rangle = \left(V^* V^T \right)_{ii'}, \quad \kappa_{ii'} = \langle \Phi | a_{i'} a_i | \Phi \rangle = \left(V^* U^T \right)_{ii'} \tag{20}$$

giving

$$E[\rho, \kappa] = \frac{\langle \Phi | H | \Phi \rangle}{\langle \Phi | \Phi \rangle} = \mathrm{Tr} \left[\left(e + \frac{1}{2} \Gamma \right) \rho \right] - \frac{1}{2} \mathrm{Tr} \left[\Delta \kappa^* \right] \tag{21}$$

where

$$\Gamma_{i_1 i_3} = \sum_{i_2 i_4} \bar{v}_{i_1 i_2 i_3 i_4} \rho_{i_4 i_2} \quad \text{and} \quad \Delta_{i_1 i_2} = \sum_{i_3 i_4} \bar{v}_{i_1 i_2 i_3 i_4} \kappa_{i_3 i_4}. \tag{22}$$

One finally obtains the Hartree-Fock-Bogolyubov equations by considering variation of the energy functional (21) with respect to ρ and κ giving:

$$\begin{pmatrix} e + \Gamma - \lambda & \Delta \\ -\Delta^* & -(e + \Gamma)^* + \lambda \end{pmatrix} \begin{pmatrix} U \\ V \end{pmatrix} = E \begin{pmatrix} U \\ V \end{pmatrix} \tag{23}$$

with a Lagrange multiplier λ correcting the average particle number.

2.4.4 Skyrme Hartree-Fock-Bogolyubov equations

The Skyrme energy functional models the effective interaction between nucleons[1]. Including Skyrme forces the energy density functional in (21) becomes [19]

$$E[\rho,\tilde{\rho}] = \int d^3\vec{r}\,\mathcal{H}(\vec{r}) \tag{24}$$

where $\tilde{\rho}$ is the local pairing density and

$$\mathcal{H}(\vec{r}) = H(\vec{r}) + \tilde{H}(\vec{r}) \tag{25}$$

is the sum of the mean-field and total pairing energy densities. The densities $H(\vec{r})$ and $\tilde{H}(\vec{r})$ depend on $\rho(\vec{r})$, $\tilde{\rho}(\vec{r})$, $\tau(\vec{r})$ and the spin current density $J_{ij}(\vec{r})$. These are the local (diagonal) densities, that are expressed as [19]:

$$\begin{aligned} \rho(\vec{r}) &= \rho(\vec{r},\vec{r}), & \tilde{\rho}(\vec{r}) &= \tilde{\rho}(\vec{r},\vec{r}), \\ \tau(\vec{r}) &= \nabla_r\nabla_{r'}\rho(\vec{r},\vec{r}')|_{\vec{r}'=\vec{r}}, & J_{ij}(\vec{r}) &= \tfrac{1}{2i}\left(\nabla_i - \nabla'_i\right)\rho_j(\vec{r},\vec{r}')|_{\vec{r}'=\vec{r}}. \end{aligned} \tag{26}$$

Where i and j are the indices of the Jacobian matrix, indicating the coordinates for the gradients and densities [11]. In this case the density matrices $\rho(\vec{r},\vec{r}')$,$\rho_i(\vec{r},\vec{r}')$, $\tilde{\rho}(\vec{r},\vec{r}')$ and $\tilde{\rho}_i(\vec{r},\vec{r}')$ are defined using the non-local versions of the density definitions [19]:

$$\begin{aligned} \rho(\vec{r}\sigma,\vec{r}'\sigma') &= \tfrac{1}{2}\rho(\vec{r},\vec{r}')\delta_{\sigma\sigma'} + \tfrac{1}{2}\textstyle\sum_i(\sigma|\sigma_i|\sigma')\rho_i(\vec{r},\vec{r}') \\ \tilde{\rho}(\vec{r}\sigma,\vec{r}'\sigma') &= \tfrac{1}{2}\tilde{\rho}(\vec{r},\vec{r}')\delta_{\sigma\sigma'} + \tfrac{1}{2}\textstyle\sum_i(\sigma|\sigma_i|\sigma')\tilde{\rho}_i(\vec{r},\vec{r}') \end{aligned} \tag{27}$$

These are the standard definitions using the spin-dependent one-body density matrices with σ indicating spin. This work only considers spin-dependent one-body density matrices allowing for the replacement of the time-odd pairing tensor κ with the time-even pairing density matrix $\tilde{\rho}(\vec{r}\sigma,\vec{r}'\sigma') = -2\sigma'\kappa(\vec{r},\sigma,\vec{r}',-\sigma')$. The final Skyrme Hartree-Fock-Bogolyubov equations resulting from variation of the energy functional (24) with respect to ρ and $\tilde{\rho}$ is then:

$$\sum_{\sigma'}\begin{pmatrix} h(\vec{r},\sigma,\sigma') & \tilde{h}(\vec{r},\sigma,\sigma') \\ \tilde{h}(\vec{r},\sigma,\sigma') & -h(\vec{r},\sigma,\sigma') \end{pmatrix}\begin{pmatrix} U(E,\vec{r}\sigma') \\ V(E,\vec{r}\sigma') \end{pmatrix} = \begin{pmatrix} E+\lambda & 0 \\ 0 & E-\lambda \end{pmatrix}\begin{pmatrix} U(E,\vec{r}\sigma) \\ V(E,\vec{r}\sigma) \end{pmatrix} \tag{28}$$

where $h(\vec{r},\sigma,\sigma')$ and $\tilde{h}(\vec{r},\sigma,\sigma')$ are local fields. The values for $h(\vec{r},\sigma,\sigma')$, $\tilde{h}(\vec{r},\sigma,\sigma')$, $H(\vec{r})$ and $\tilde{H}(\vec{r})$ and be expressed and calculated explicitly, the explicit expressions considered in this work can be found in the HFBTHO program article[19].

3 METHOD

For repeat ability purposes and further insight into the specifics of the origin of the results this section will describe parameters used for the HFBTHO program.

3.1 HFBTHO program and application

The HFBTHO program solves the nuclear many body problem numerically by applying the above Skyrme Hartree-Fock-Bogolyubov equations (28). There have been different approaches for obtaining numerical solutions such as the two basis method in which the canonical basis is constructed through a combination of the imaginary-time evolution method and a diagonalization of the Hartree-Fock-Bogolyubov Hamiltonian matrix[28]. The HFBTHO program instead expands the Hartree-Fock-Bogolyubov solution to the basis of either a harmonic oscillator or transformed harmonic oscillator. For the work performed in this thesis we use version 2.00d of the HFBTHO program which applies additional corrections[18]. After compiling and preparing the program, an input file is used to specify the parameters for the program. These parameters are shown in table II. Explanations for the default parameters can be found in the HFBTHO v2.00d publication[18] while the parameters varied for this work will be discussed here.

The *number_of_shells* parameter is used to specify the number of shells used in for the calculations, where the number of states in the Harmonic oscillator basis equals to $(N_{sh}+1)(N_{sh}+2)(N_{sh}+3)/6$ as defined by the program. 14 was chosen as a compromise between run time and accuracy as the run time of the program increases polynomially with the increase in number of shells. The *proton_number* and *neutron_number* parameters specify which nuclei the program is run on. The *number_iterations* and *accuracy* parameters where increased and decreased respectively to improve precision of results. The *add_initial_pairing* parameter was set to True to ensure pairing correlations remain non-zero. The *set_temperature* and *temperature* parameters were changed as investigation into their effects found the default value 0 caused a sharp increase in computation time without significantly improving results[5].

HFBTHO_GENERAL		
number_of_shells = 14	oscillator_length = -1.0	basis_deformation = 0.0
proton_number = 24	neutron_number = 26	type_of_calculation = 1
HFBTHO_ITERATIONS		
number_iterations = 400	accuracy = 1.E-6	restart_file = -1
HFBTHO_FUNCTIONAL		
functional = 'SLY4'	add_initial_pairing = T	type_of_coulomb = 2
HFBTHO_PAIRING		
user_pairing = F	vpair_n = -300.0	vpair_p = -300.0
pairing_cutoff = 60.0	pairing_feature = 0.5	
HFBTHO_CONSTRAINTS		
lambda_values = 1, 2, 3, 4, 5, 6, 7, 8		
lambda_active = 0, 0, 0, 0, 0, 0, 0, 0		
expectation_values = 0.0, -1.7 , 0.0, 0.0, 0.0, 0.0, 0.0, 0.0		
HFBTHO_BLOCKING		
proton_blocking = 0, 0, 0, 0, 0	neutron_blocking = 0, 0, 0, 0, 0	
HFBTHO_PROJECTION		
switch_to_THO = 0	projection_is_on = 0	gauge_points = 1
delta_Z = 0	delta_N = 0	
HFBTHO_TEMPERATURE		
set_temperature = T	temperature = 0.04	
HFBTHO_DEBUG		
number_Gauss = 40	number_Laguerre = 40	number_Legendre = 80
compatibility_HFODD = F	number_states = 500	force_parity = T
print_time = 0		

TABLE II: Table showing parameters of input file for HFBTHO program where non-highlighted values are default and highlighted values are changed for this work

Finally the second value of the *expectation_values* parameter was varied between:

$$-10\frac{0.4e^{ln(A)\times 1.3333}}{110} \quad \text{and} \quad 10\frac{0.4e^{ln(A)\times 1.3333}}{110} \tag{29}$$

for each nucleus to obtain results for different deformations of the nucleus. These values where chosen based on previous investigation finding that they produced a good range of deformations[5]. A parameter that is kept as default but can have a large effect on the program is the $functional$ parameter which designates which Skyrme functional is used. In this case the Sly4 (Skyrme Lyon 4) interaction is used as it is well tested and is improved by the neural network in a nice way. Another potential choice would be the UNEDF1 interaction which can be better for describing binding energies[2].

4 RESULTS

4.1 Initial neutron drip-line prediction

As the HFBTHO program is computer resource intensive and it needs to be applied to a large number of nuclei, it is helpful to have an initial prediction for the neutron drip-line location. This will allow for a more informed choice for which nuclei one needs to apply the program to. Figure 4 shows the prediction made with a neural network trained to reproduce experimental binding energy values with only neutron number and proton number as inputs. The produced figure provides a reference point for more trusted future methods along with an initial estimate for neutron drip-line location.

The figure was produced by running multiple instances of the neural network each producing a model used to predict the neutron drip-line location. For every model the root mean square standard deviation between the model's predicted binding energies and the experimental values is obtained and considered to be the model error. The model with lowest model error is then considered the best model while the error bars for this model are obtained using an error approximation method. This error approximation method functions by sampling a set containing all models with a model error equal to or less than twice the best model error, then for each proton number the lowest and highest neutron number locations of the drip-line from the sampled set are plotted as the error bars. For each of the figures the neural network was run 100 times producing 100 predictions for the neutron drip-line location.

It can be seen that when trained without theoretical results there is a large variance in neutron drip-line location for different models shown by the wide error estimate in figure 4. This makes this form of prediction unhelpful for determining the location of the drip-line. However, it remains useful as a point of comparison. The aspects interesting for comparison are the distribution of deviation from experimental results, the total root mean square deviation of 4.66MeV and the width of the error approximation obtained.

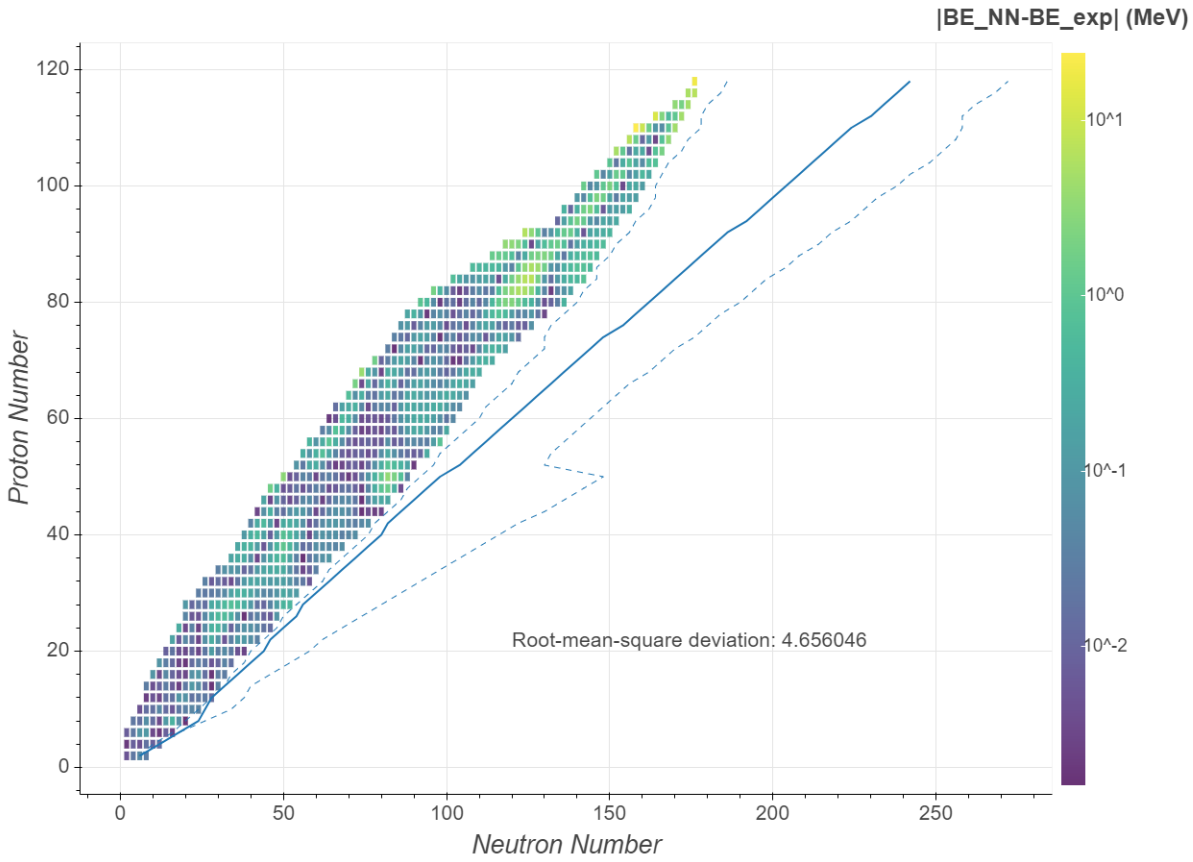

FIG. 4: Location of neutron drip-line along with error estimation predicted by neural-network without theoretical values, the blue line is the prediction while the dashed blue line is the error estimation. The even-even nuclei with experimental data are shown along with the difference between the best model's predicted binding energy and the experimental data for each of these nuclei

4.2 HFBTHO predicted neutron drip-line

In figure 4, 86 of the 100 models had a root mean square deviation less then or equal to twice the best model and where used for the error bars. With a general estimate for the upper bound of potential neutron drip-line locations the HFBTHO program was run for the 859 AME16 available experimental even-even nuclei together with 3944 even-even nuclei to the right of the experimental data to find the drip-line. The difference between these theoretical results and experimental data along with predicted neutron drip-line location are shown in figure 5. The line produced has no error approximation as rather than the

location of the drip-line this result should be interpreted as the location of the drip-line as calculated by the HFBTHO model with the discussed parameters.

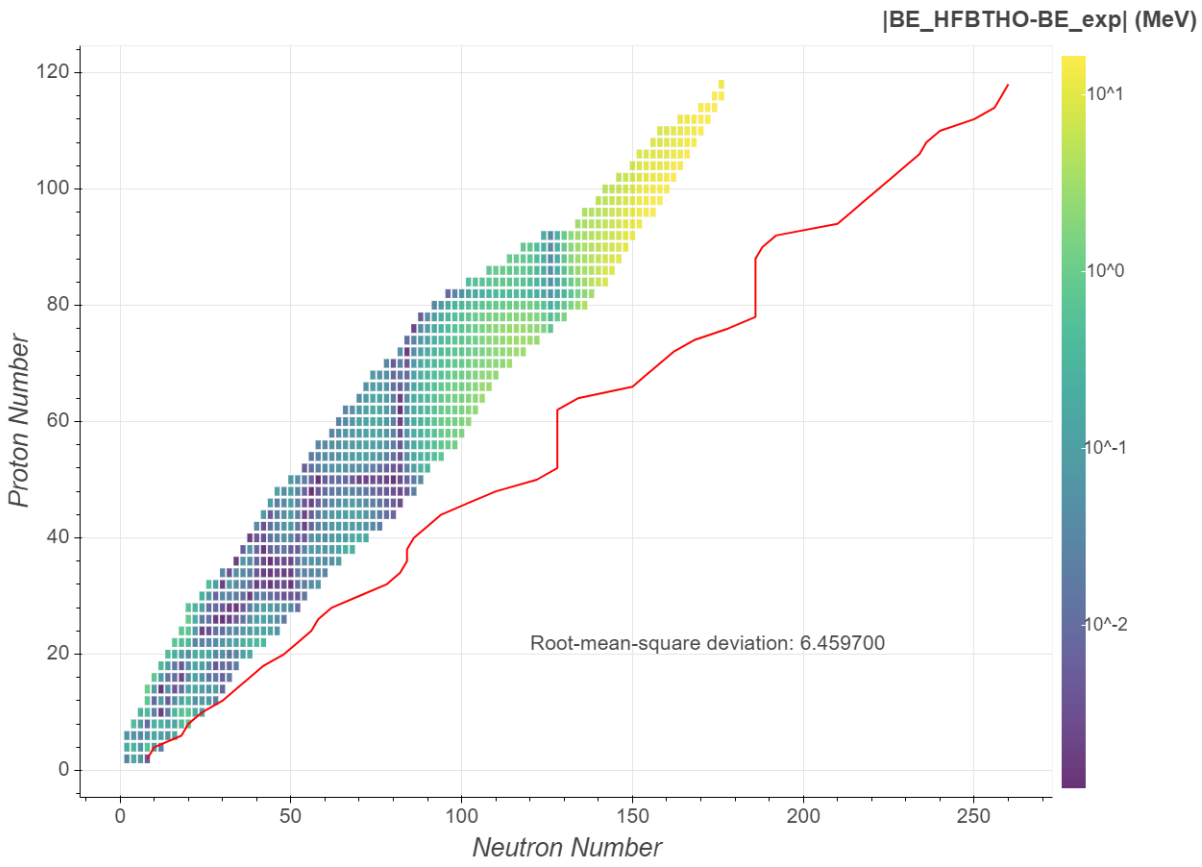

FIG. 5: The location of neutron drip-line predicted by theoretical HFBTHO solutions using the Sly4 interaction is shown with a red line. The even-even nuclei with experimental data are shown along with the difference between the HFBTHO solved binding energies and the experimental data for each of these nuclei

Observing the resulting deviation distribution in figure 5 it is visible that while being good for low nucleon numbers the theoretical values get worse as the nucleon number increases. An exception to this seems to be the magic numbers where the theoretical values again approach experimental ones. The most likely source for this increase in deviation is the number of shells parameter when performing HFBTHO calculations. The importance of a sufficiently large value for the parameter increases as the mass number A increases. For low values of A the number_of_shells = 14 produces good results for the HFBTHO program while as A increases a larger value is required. Ideally a larger value for the number_of_shells

parameter would be chosen such as 20 or 25 however the polynomial increase in computing time as the parameter increases is a limiting factor[11].

For reference the predictions by the initial prediction network and theoretically produced values of neutron drip-line location are shown in figure 6.

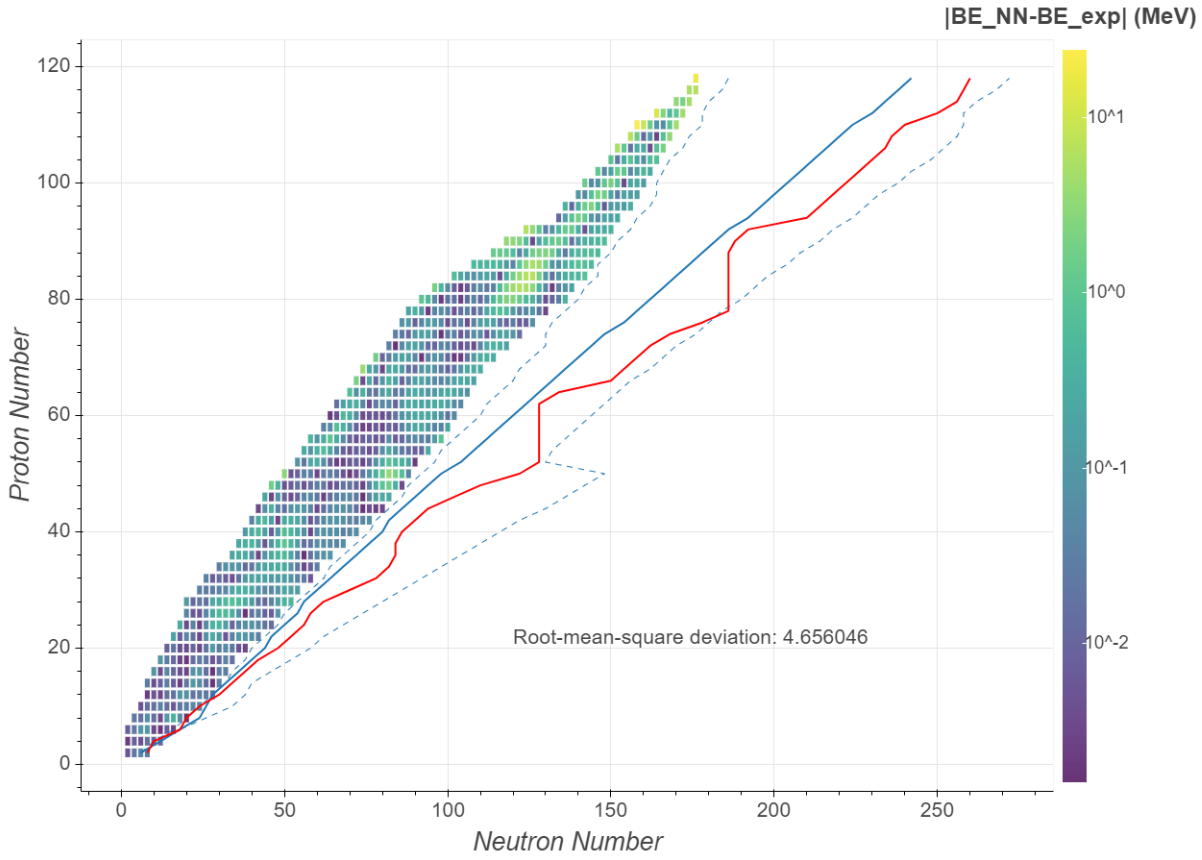

FIG. 6: Location of the neutron drip-line along with error estimation by neural-network. (see main text for details) Red solid lines: theoretical neutron drip-line from HFBTHO. Purple lines neural network prediction for the neutron drip-line (solid) and error approximation (dashed). Additionally the even-even nuclei with experimental data are shown along with the difference between the best model's predicted binding energy and the experimental data for each of these nuclei

Observing the result one can see that the theoretical results fit quite well within the error bars of the basic network predictions.

4.3 Improved neural network neutron drip-line prediction

Figure 7 shows the neural network with only proton and neutron numbers as input but trained to reduce the difference between HFBTHO values and the experimental values.

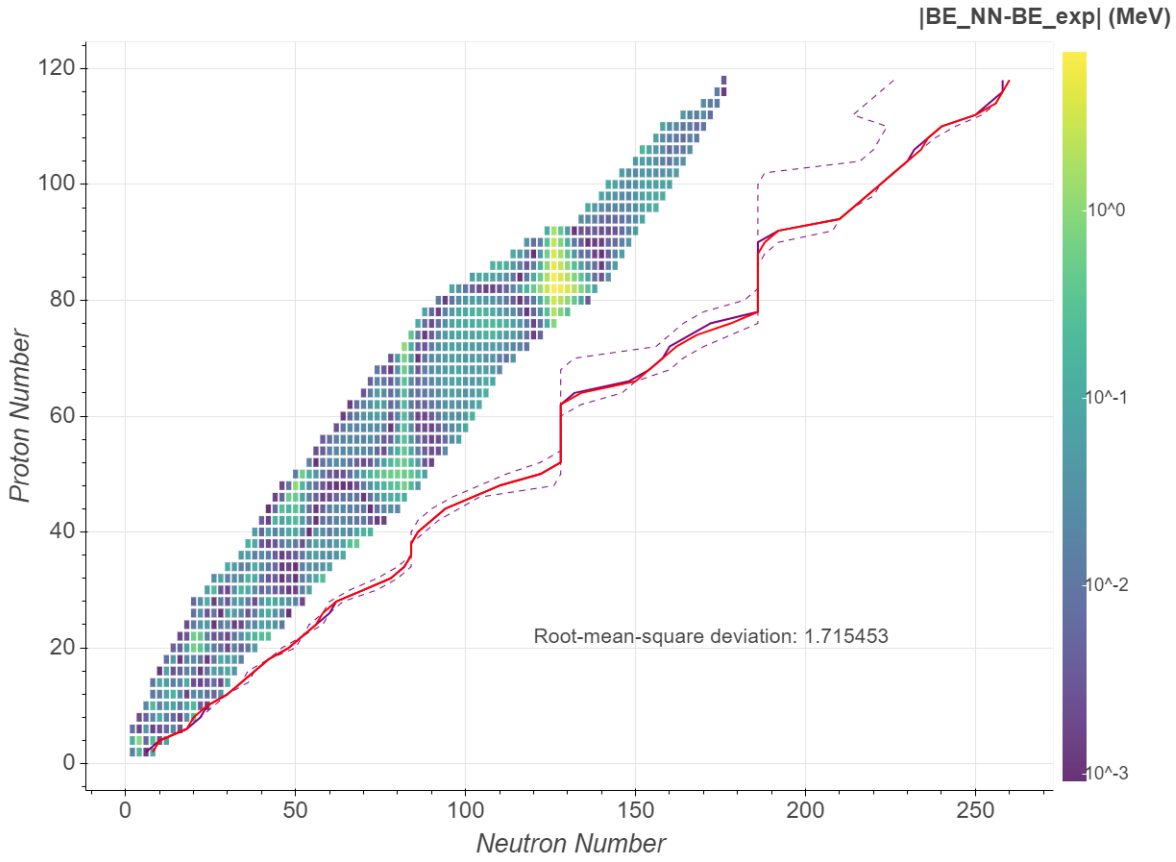

FIG. 7: Location of the neutron drip-line along with error estimation by neural-network. (see main text for details) Red solid lines: theoretical neutron drip-line from HFBTHO. Purple lines neural network prediction for the neutron drip-line (solid) and error approximation (dashed). Additionally the even-even nuclei with experimental data are shown along with the difference between the best model's predicted binding energy and the experimental data for each of these nuclei

In figure 7 all 100 of the 100 models had a root mean square deviation less then or equal to twice the best model and where used for the error bars. Comparing the results with figure 6 one can see an immediate improvement in both the variation in drip-line location and root mean square deviation. Another thing to note concerns the distribution of deviation around the magic numbers, here the deviation from experimental results is worse than the pure HFBTHO results in figure 5, this is visible by looking at the regions around $Z = 50$ to

$Z = 70$ at $N = 82$ and $Z = 82$ at $N = 126$. The cause of this is likely slight over-correction by the neural network in these regions.

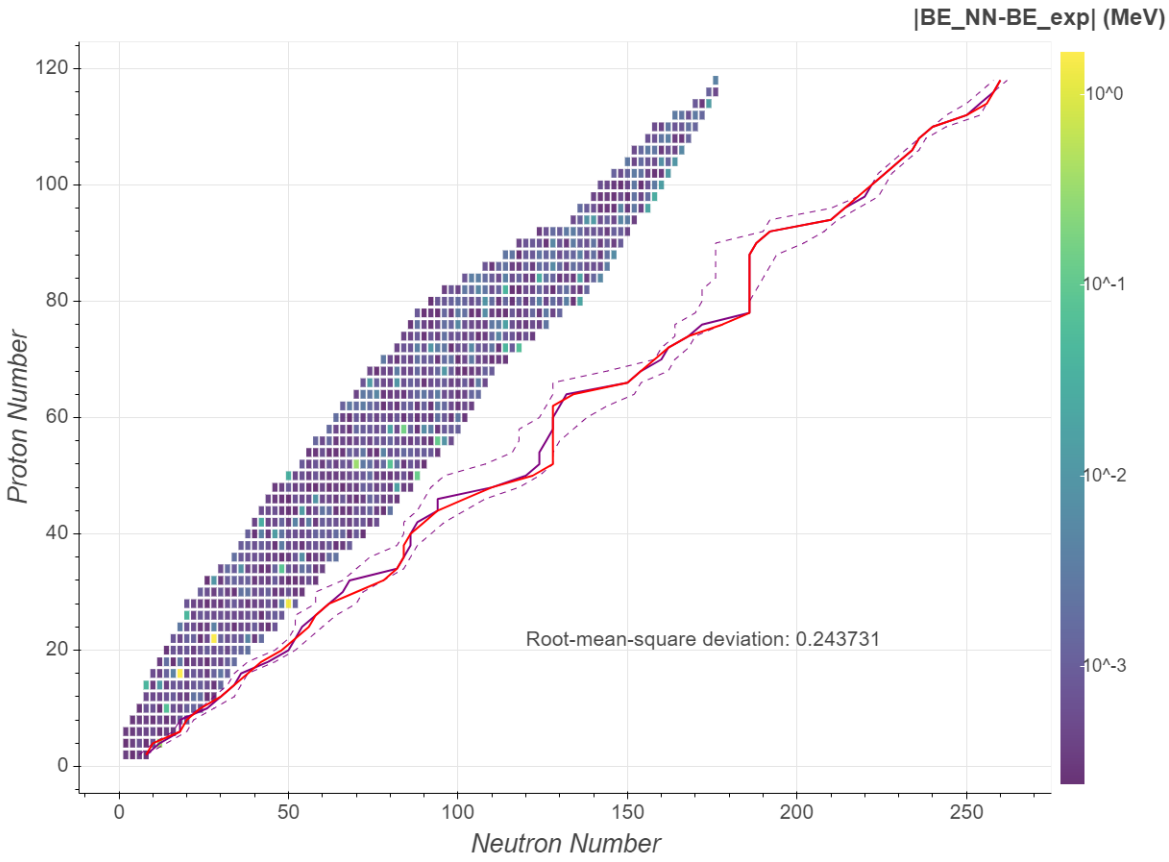

FIG. 8: Location of the neutron drip-line along with error estimation by neural-network. (see main text for details) Red solid line: theoretical neutron drip-line from HFBTHO. Purple lines neural network prediction for the neutron drip-line (solid) and error approximation (dashed). Additionally the even-even nuclei with experimental data are shown along with the difference between the best model's predicted binding energy and the experimental data for each of these nuclei

Finally figure 8 shows the neural network results for a network that takes proton number, neutron number, deformation, neutron pairing energy and proton pairing energy as inputs and trains to reduce the difference between HFBTHO results and experimental results. 21 deformations between approximately -0.5 and 0.5 where used along with the correlating pairing energies for each deformation.

Again in figure 8 all 100 of the 100 models had a root mean square deviation less then or

equal to twice the best model and where used for the error bars. The inclusion of pairing energies for different deformations was of interest due to the importance the HFBTHO program places on pairing correlation when determining binding energies. The results in figure 8 show considerable improvement in root mean square deviation being an order of magnitude better than previous results. An unfortunate side effect however is that the produced drip-line does not seem to be as affected by the magic numbers as the results in 7 which was an expected property of a good drip-line prediction.

These final results show an improvement of 96.21% in the root mean square deviation indicating the effectiveness of the application of neural networks in recreating experimental results. The final root mean square deviation of 0.245MeV is also of a similar order of magnitude to Bayesian neural network approaches performed [22]. The predicted drip-line location also correlates well with the obtained theoretical drip-line location. There remain however aspects of this work that could be improved to improve the results. The neural networks applied in this work function by applying corrections to the results produced by the HFBTHO program, increasing the accuracy of these theoretical results would increase the trustworthiness of the drip-line prediction. This is especially important for the final method producing figure 8 where more HFBTHO data is included in the training of the network. The main improvement would come from and increase in the number_of_shells parameter. This would require setting aside far more time for the obtaining of HFBTHO values however is especially important for the neutron drip-line calculations where the high number of neutrons are less bound and require more shells to be modeled correctly. Also due to requiring a value of 20 or greater for the number_of_shells parameter to function correctly the transformed harmonic oscillator basis was not used in this work, with the increase in number_of_shells this basis could be used. Finally there exists a third version of the HFBTHO program which applies additional corrections and could be used to improve accuracy. Examples of changes made in the newer version are, inclusion of the full Gogny force and calculation of the nuclear collective inertia [23]. Additional improvements could also be made to the final neural network setup, for example 1000 nodes in one hidden layer was chosen for the neural network node setup based on hyperparameter optimization done by A. Idini[10]. However this optimisation was done with input and training sets similar to figure 4 with only neutron and proton numbers as input and trained without theoretical data. An

additional hyperparameter optimization could be done for networks with additional inputs based on HFBTHO data in order to determine a better hidden node setup. Additionally normalisation of input parameters could be improved and further investigation into which input parameters that could be included produce the best effects could be conducted.

The method of producing the results in figure 8 was repeated for the proton drip-line for figure 9 in order to apply the most successful method in making a prediction for the proton drip-line as well.

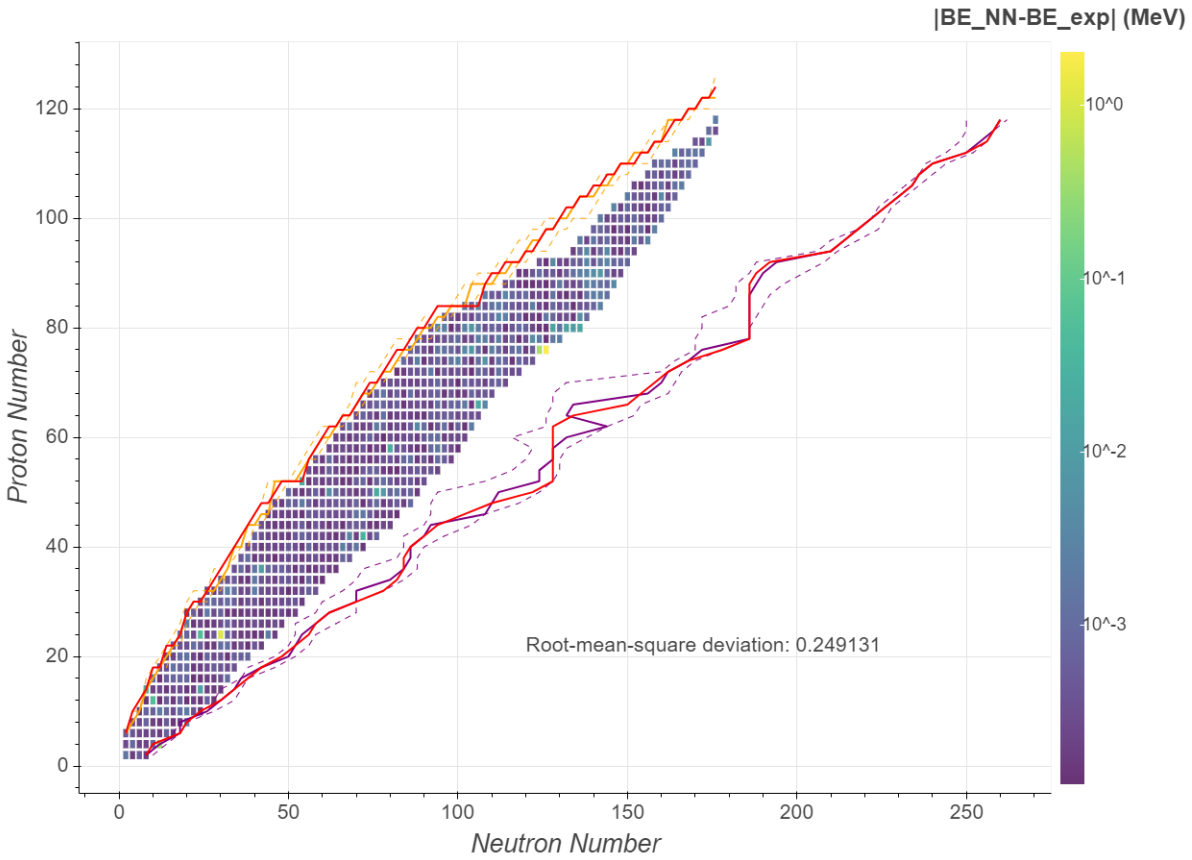

FIG. 9: Location of the n and p drip-lines along with error estimation by neural-network. (see main text for details) Red solid lines: theoretical p- and n- drip-lines from HFBTHO. Purple lines neural network prediction for the n- drip-line (solid) and error approximation (dashed). Orange lines: same as for purple but p- drip-line. Additionally the even-even nuclei with experimental data are shown along with the difference between the best model's predicted binding energy and the experimental data for each of these nuclei

5 SUMMARY AND OUTLOOK

This work is an investigation into the application of neural networks in making predictions for both nuclear binding energies and the neutron and proton drip-line locations. The results in this work can be largely gathered into three investigations, the effectiveness of simple prediction methods, improvements that can be made for better predictions and final drip-line predictions.

Two initial predictions where made, one through applying a basic neural network setup, and the other made by applying theoretical results from the HFBTHO program. The basic network was trained to reproduce experimental results taking proton and neutron numbers as input and achieved a root mean square standard deviation from experimental results of 4.656MeV. The theoretical predictions achieved a root mean square standard deviation from experimental results of 6.460MeV. The fact that the neural network was able to more closely reproduce experimental results than the HFBTHO program indicated the potential for network application in predicting experimental results.

With initial predictions made the neural network was improved by providing theoretical information to the neural network in two different ways. First the network was trained to decrease the difference between theoretical and experimental results by applying a correction, this network still only took proton and neutron numbers as input and achieved a root mean square standard deviation from experimental results of 1.715MeV. Another improvement was made to this network by increasing the number of inputs, by providing the network input information about the pairing energies of the neutrons and protons for different nuclei deformations the network achieved a root mean square standard deviation from experimental results of 0.244MeV. The inclusion of theoretical values in neural network training improved deviation from experimental results by an order of magnitude indicating the validity of this method of binding energy prediction.

With a network setup chosen predictions where made for the proton and neutron drip-line locations, these predictions are shown in figure 9. These results can provide a reference point for future investigations in the regions of the drip-lines. The results achieved also provide evidence for the application of neural networks being a reasonable option for making predictions within nuclear physics.

There exist several potential directions for further investigation including methods of improving the current results and additional applications for the methods applied in this work. The current results could be improved through an increase in the number_of_shells parameter of the HFBTHO program increasing the accuracy of theoretical values for larger nuclei. Use of a newer version of the program and the application of a transformed harmonic oscillator basis are alternative routs for theoretical value improvements. Additionally investigation into other programs that apply theoretical models to obtain theoretical results could be done. Further improvements could be made the the choice of hidden nodes of the neural network by performing additional hyperparameter optimization. Finally the methods applied here could be applied in the investigation of Q-alpha values for super heavy nuclei. Similarly to predicting the neutron drip-line, by expanding the region where HFBTHO values are calculated it would be possible to use the networks from this work to make Q-alpha value predictions.

REFERENCES

[1] Bender, M., Heenen, P., and Reinhard, P., Rev. Mod. Phys. **75**, 121 (2003).

[2] Carlsson, G., Private Communication (2020).

[3] Cartwright, H., *Artificial Neural Networks* (Springer, New York, NY).

[4] Chollet, F. *et al.*, "Keras," (2015).

[5] Cui, W., Private Communication (2020).

[6] Gales, S., Nuclear Physics A **834**, 717c (2010), the 10th International Conference on Nucleus-Nucleus Collisions (NN2009).

[7] Hagino, K., Tanihata, I., and Sagawa, H., 100 Years of Subatomic Physics , 231–272 (2013).

[8] Hartree, D. R., Mathematical Proceedings of the Cambridge Philosophical Society **24**, 89–110 (1928).

[9] Huang, W., Audi, G., Wang, M., Kondev, F., Naimi, S., and Xu, X., Chinese Physics C **41**, 030002 (2017).

[10] Idini, A., "Statistical learnability of nuclear masses," (2019), arXiv:1904.00057 [nucl-th].

[11] Idini, A., Private Communication (2020).

[12] Isao Tanihata, Daisy Hirata, T. K. S. S. K. S. and hiroshi toki,, Physics Letters B **289**, 261 (1992).

[13] Jochen Erler, Noah Birge, M. K. W. N. E. O. A. P. M. S., Nature **486**, 1930008 (2012).

[14] Jonson, B., Herald of the Russian Academy of Sciences **89**, 221–230 (2019).

[15] Kruecken, R., CONTEMPORARY PHYSICS **52**, 101 (2011).

[16] Lattimer, J. M. and Prakash, M., **442**, 109 (2007), arXiv:astro-ph/0612440 [astro-ph].

[17] Lions, P. L. and Gogny, D., ESAIM: M2AN **20**, 571 (1986).

[18] Mario Stoitsov, Nicolas Schunck, M. K. N. M. H. N. E. O. J. S. and Wild, S., Computer Physics Communications **184**, 1592–1604 (2013).

[19] Mario Stoitsov, Jacek Dobaczewski, W. N. and Ring, P., Computer Physics Communications **167**, 43–63 (2005).

[20] Nakada, H., International Journal of Modern Physics E , 1930008 (2020).

[21] Nakamura, T., Few-Body Systems **54**, 857 (2013).

[22] Niu, Z. and Liang, H., Physics Letters B **778**, 48 (2018).

[23] Perez, R. N., Schunck, N., Lasseri, R.-D., Zhang, C., and Sarich, J., Computer Physics Communications **220**, 363 (2017).

[24] Sherrill, D. and Schaefer, H. F. (Academic Press, 1999) pp. 143 – 269.

[25] Tanihata, I., Hamagaki, H., Hashimoto, O., Shida, Y., Yoshikawa, N., Sugimoto, K., Yamakawa, O., Kobayashi, T., and Takahashi, N., Phys. Rev. Lett. **55**, 2676 (1985).

[26] Tanihata, I., Hirata, D., Kobayashi, T., Shimoura, S., Sugimoto, K., and Toki, H., Physics Letters B **289**, 261 (1992).

[27] Wang, M., Audi, G., Kondev, F., Huang, W., Naimi, S., and Xu, X., Chinese Physics C **41**, 030003 (2017).

[28] Yamagami, M., Matsuyanagi, K., and Matsuo, M., Nuclear Physics A **693**, 579 (2001).

APENDIX A: SPECIFIC NEURAL NETWORK

The neural network used in this this work applies the python programming library Keras based on Tensorflow[4]. In this work the applied neural network was configured in the following way:

The number of input and output nodes where taken as 50 and 1 respectively, allowing for the input of multiple characteristics obtained from the HFBTHO program while only the resulting binding energy is of interest in this work.

The number of hidden layers and nodes per hidden layer where chosen as 1 and 1000 respectively, this choice correlates with an investigation into the validity of neural network use in binding energy predictions by A. Idini[10].

The epochs, referring to the number of iterations allowed when minimizing the loss function was chosen as 2500.

The activation function used for input layers was a “sigmoid” activation function while a ”ReLU” activation function was used for the hidden layer.

Due to the low number of hidden layers no dropout was used leaving dropout rate as zero.

The weights and biases were initialised by taking random numbers with a mean value of 0 and standard deviation of 0.05. This varied the starting point of the network causing multiple runs to result in different final weights, alowing for the reduction of the importance of starting weights in the final predictions

The RMSprop optimizer was chosen for use as optimizer.

For cross validation 10 sets where used where the Python library scikit-learn was used for the data processing in cross validation.

The experimental data used in training and comparison comed from the 2016 atomic mass evaluation or AME16[9][27].

APENDIX B: ADDITIONAL HFBTHO PROGRAM INFORMATION

This Apendix will go give a short description of the parameters of the HFBTHO program which where not discussed in the main text where descriptions where obtained from the HFBTHO v2.00 documentation [18]. The *oscillator_length* parameter allows fer the input of a desired oscillator length in fm.

The *basis_deformation* parameter allows for the axial deformation of the basis with only axial quadrupole deformations possible, negative values correspond to an oblate basis.

The *type_of_calculation* paramiter defines the type of calculation to be performed where 1 signifies standard HFB calculations and for -1 the code will approximate particle-number projection by the Lipkin-Nogami prescription.

The *restart_file* parameter determines whether the calculation will begin from an existing solution (-1) or begin by solving the Schrödinger equation for a Woods-Saxon potential (1).

The *type_of_coulomb* parameter determines the Coulomb potential is considered, with 0 representing no direct or exchange term, 1 representing only the direct term and 2 representing the inclusion of both the direct and exchange terms.

The *user_pairing* paramiter when set to true (T) aloes the user to set some charactaristics of the paring interaction.

The *vpair_n* parameter sets the value of the pairing strength (in MeV) for neutrons.

The *vpair_p* parameter sets the value of the pairing strength (in MeV) for protons.

The *pairing_cutoff* parameter sets the energy cutoff (in MeV) where all quasiparticles with energy lower than the cutoff are taken into account in the calculation of densities.

The *pairing_feature* parameter enables one to tune the properties of the pairing force where for value 0 the pairing force has pure volume character, for value 1 the pairing force is only active at the surface and inbetween 0 and 1 the pairing force has mixed volume-surface characteristics.

The *lambda_values* are a series of 8 integers which define the multipolarity of the multipole moment constraints.

The *lambda_active* parameters defines which of the multipole moments operators will be used as constraints.

The *expectation_values* parameters specifies the value of the constraint for each multipolarity.

The *proton_blocking* and *neutron_blocking* parameters determine the blocking configuration for protons and neutrons respectively.

The *switch_to_THO* parameter controls the use of the transformed harmonic oscillator basis.

The *projection_is_on* parameter determines whether or not particle number projection (after variation) is used.

The *gauge_points* parameter determines the number of gauge points used in particle number projection.

The *delta_Z* and *delta_N* parameters specify the values for δZ and δN used for HFB result projection if particle projection is on.

The *number_Gauss* and *number_Laguerre* parameters specify the number of Gauss-Hermite and Gauss-Laguerre integration points for integrations along the elongation and perpendicular axis respectively.

The *number_Legendre* determines the number of Gauss-Legendre integration points for the calculation of the direct Coulomb potential.

The *compatibility_HFODD* parameter enforces the same HO basis as in HFODD when set to true. The *number_states* parameter is used when compatibility with HFODD is enforced and determines the total number of states in the basis.

The *force_parity* parameter when set to true enforces the conservation or breaking of parity depending on the multipolarity of the multipole moments used as constraints.

Finally the *print_time* can be used to display the time taken by some of the major routines.